



Article

# Apolipoprotein E (ApoE) Rescues the Contractile Smooth Muscle Cell Phenotype in Popliteal Artery Aneurysm Disease

Jessica Pauli <sup>1,2</sup> , Tessa Reisenauer <sup>1</sup>, Greg Winski <sup>3,4</sup> , Nadja Sachs <sup>1,2</sup> , Ekaterina Chernogubova <sup>3</sup>, Hannah Freytag <sup>1</sup>, Christoph Otto <sup>5</sup>, Christian Reeps <sup>6</sup>, Hans-Henning Eckstein <sup>1,2</sup>, Claus-Jürgen Scholz <sup>7</sup> , Lars Maegdefessel <sup>1,2,3</sup> and Albert Busch <sup>1,6,\*</sup>

<sup>1</sup> Department for Vascular and Endovascular Surgery, Klinikum rechts der Isar, Technical University Munich, 81675 Munich, Germany

<sup>2</sup> German Center for Cardiovascular Research (DZHK), Partner Site Munich Heart Alliance, 10785 Berlin, Germany

<sup>3</sup> Molecular Vascular Medicine Group, Center for Molecular Medicine, Karolinska Institute, 17177 Stockholm, Sweden

<sup>4</sup> Perioperative Medicine and Intensive Care, Karolinska University Hospital, 17177 Stockholm, Sweden

<sup>5</sup> Department of General, Visceral, Transplantation, Vascular & Pediatric Surgery, University Hospital Würzburg, 97080 Würzburg, Germany

<sup>6</sup> Division of Vascular and Endovascular Surgery, Department for Visceral, Thoracic and Vascular Surgery, Medical Faculty Carl Gustav Carus and University Hospital, Technische Universität Dresden, 01307 Dresden, Germany

<sup>7</sup> Wispliinghoff Laboratories, 50858 Cologne, Germany

\* Correspondence: albert.busch@uniklinikum-dresden.de; Tel.: +49-351-458-3072



**Citation:** Pauli, J.; Reisenauer, T.; Winski, G.; Sachs, N.; Chernogubova, E.; Freytag, H.; Otto, C.; Reeps, C.; Eckstein, H.-H.; Scholz, C.-J.; et al. Apolipoprotein E (ApoE) Rescues the Contractile Smooth Muscle Cell Phenotype in Popliteal Artery Aneurysm Disease. *Biomolecules* **2023**, *13*, 1074. <https://doi.org/10.3390/biom13071074>

Academic Editor: Adriana Georgescu

Received: 12 April 2023

Revised: 22 June 2023

Accepted: 28 June 2023

Published: 4 July 2023



**Copyright:** © 2023 by the authors. Licensee MDPI, Basel, Switzerland. This article is an open access article distributed under the terms and conditions of the Creative Commons Attribution (CC BY) license (<https://creativecommons.org/licenses/by/> 4.0/).

## 1. Introduction

Aneurysm formation is most often seen and has been best investigated for the ascending aorta and specifically the infrarenal abdominal aortic aneurysm (AAA). The most frequent peripheral aneurysm and a common concern in vascular surgery is the popliteal artery aneurysm (PAA). Its prevalence is about 1% in the susceptible population (male smokers, aged > 55) and occurs bilaterally upon diagnosis in more than 50% of cases [1]. Approximately half of the affected patients show at least one further aneurysm, most often in the aorta [2,3].

Despite a similar population, clinical symptoms are distinct. The rupture rate is low and complications are mainly caused by leg ischemia, due to silent onset longtime or acute peripheral embolism or local compression resulting in acute leg ischemia, deep vein thrombosis or popliteal fossa pain [4]. This has led to a vivid ongoing discussion about treatment indication and modality. Currently, open repair by local aneurysm exclusion or bypass is favored over endovascular covered stent implantation [5,6]. Generally, indications for elective repair are a maximum diameter >20 mm, luminal thrombus load and possible eccentric morphology [4,7–9]. Occurrence is occasionally within defined clinical syndromes (e.g., Loeys-Dietz syndrome) or rheumatoid vasculitis (e.g., Behcet's disease) or exostoses, causing eventual mechanic vessel irritation [10–13]. In most cases, PAA should be considered a distinct entity with a widely unknown pathogenesis [9].

This might be due to the specific anatomic niche with constant movement in at least two axis and the muscular type artery origin with a possible different susceptibility to external stimuli in comparison to elastic type arteries, such as the aorta [14]. Nevertheless, PAA samples show features of degenerative vascular wall remodeling [15,16]. This was mainly investigated compared to characteristics of AAA and is equally lacking hints of the initial cause for diameter enlargement [17]. Here, in the so-called VSMC phenotype switch, the loss of contractile characteristics is a pathogenic hallmark and phenotype rescue is a proposed salvage mechanism to halt AAA growth [18–20]. Furthermore, trans-differentiation to other cell types has been described, once the senescent phenotype is lost [19,21].

Specifically for PAA, neutrophil and T<sub>H</sub>1-cell rich infiltrates and upregulation of proteolytic matrix metalloproteinases (MMP), and cathepsins have been observed in tissue samples [22,23]. Additionally, loss of contractile elements and macrophage infiltration has been described by others and us [16,23,24]. Apart from that, little is known about specific pathomechanisms involved in PAA development and progress, yet severe atherosclerosis is concomitantly observed in most patients. In the present study, we aimed to investigate specific features of PAA in comparison to non-aneurysmatic popliteal arteries based on histologic examination, RNA profiling and cell culture experiments to identify and modify potential mechanisms distinct to AAA or atherosclerosis.

## 2. Materials and Methods

**Tissue acquisition:** Tissue acquisition was in accordance with the declaration of Helsinki, with approval of the local ethic review committee (University of Würzburg 20181107\_02; Technical University Munich: 2799/10) and with patients informed and written consent. If possible, PAAs were collected with an adjacent non-aneurysmatic vessel via a medial surgical approach.

All patients were operated on due to acute or critical limb ischemia for peripheral arterial occlusive disease (PAOD) or on preemptive means when a threshold of 20 mm diameter was reached for PAA. Tissue was immediately rinsed in PBS and divided for formalin fixation (3.5% formaldehyde, Fischer, Achern-Fautenbach, Germany) and snap freezing in liquid nitrogen. Detailed patient characteristics and numbers of samples are shown in Table S1.

AAA and PAOD tissue samples were available for comparative purposes from the Munich Vascular Biobank as previously described in extenso [25]. Briefly, samples from intraoperative specimen were treated in the same way as PAA samples described here.

**Primary cell culture:** Primary human popliteal artery SMCs from patients were isolated from PAA biopsies, harvested during surgical repair and stored in complete DMEM/F12 Medium (Sigma Aldrich, Taufkirchen, Germany) containing 5% Fetal Bovine Serum (Gibco, Thermo Fisher Scientific) and 1% Pen-Strep (Gibco, Thermo Fisher Scientific, Darmstadt, Germany). The tissue was placed in a sterile petri dish and washed with PBS (Gibco, Thermo Fisher Scientific). Adventitia was removed, and the remaining media was cut into small pieces using a sterile scalpel. The pieces of tissue were placed in digestion medium (1.4 mg/mL Collagenase A, Roche, Mannheim, Germany, in complete DMEM/F12 Medium)

in a humidified incubator at 37 °C and 5% CO<sub>2</sub> for 4–6 h. Cells were strained using a 100 µm cell strainer to remove debris. After 2 washing steps (centrifuge 400 g, 5 min; discard supernatant, re-suspended in 15 mL complete DMEM/F12 Medium) cells were re-suspended in 7 mL complete DMEM/F12 Medium and placed in a small cell culture flask in a humidified incubator at 37 °C and 5% CO<sub>2</sub>. Upon confluence, cells were stored in liquid nitrogen or processed immediately.

Primary human aortic artery smooth muscle cells (hAoSMCs) were obtained from PeloBiotech (#PB-CH-280-2011) and cultured in Smooth Muscle Cell Growth Medium (PeloBiotech, Munich, Germany), following manufacturer's instructions. These cells served as control for all cell-based assays.

All cells are (isolated and commercially available ones) are cultured in Smooth Muscle Cell Growth Medium (PeloBiotech, Munich, Germany), following manufacturer's instructions. All cells are used until passage 7.

HE staining, light microscopy and digital image acquisition: 2-µm sections of paraffin-embedded samples were mounted on Superfrost© slides (Menzel, Gießen, Germany) and stained with hematoxylin/eosin (HE) and Elastica van Gieson according to the manufacturer's protocol. Slides were digitalized with a NanoZoomer 2.0-HT Digital slide scanner: C9600© and pictures were taken with the NDP.view2© software (both Hamamatsu, Kyoto, Japan).

Immunohistochemistry: For immunohistochemistry (IHC), sections were mounted on 0.1% poly-L-lysine (Sigma-Aldrich, St. Louis, MO, USA) pre-coated SuperFrost Plus slides (Thermo Fisher Scientific, Waltham, MA, USA). For antigen retrieval the slides boiled in a pressure cooker with 10 nM citrate buffer (distilled water with citric acid monohydrate, pH 6.0) and endogenous peroxidase activity was blocked with 3% hydrogen peroxide. Samples were blocked with 10% goat serum and then incubated with primary antibodies diluted in Dako REAL Antibody Diluent (Dako, Glostrup, Denmark). Slides were then treated with biotinylated secondary antibodies and target staining was performed with peroxidase-conjugated streptavidin and DAB chromogen (Dako REAL EnVision Detection System Peroxidase/DAB+, Rabbit/Mouse Kit; Dako, Glostrup, Denmark). Mayer's hematoxylin (Carl Roth, Karlsruhe, Germany) was used for counterstaining, with appropriate positive and negative controls for every target antibody. All slides were scanned with Aperio AT2 (Leica, Wetzlar, Germany) and images were taken with the Aperio ImageScope software (version: 12.3, Leica, Wetzlar, Germany).

Antibody list: ApoE 1:800 (ab52607 abcam), SMA 1:200 (M0635 Dako), CD68 1:2000 (M0814 Dako), Ki67 1:50 (ab16667 abcam), SMA 1:200 (ab5694 abcam), vimentin 1:200 (ab8978 abcam), desmin 1:100 (ab32362 abcam).

Ki67-positive cell counting: For assessment of proliferation rates in the aneurysm and vessel wall, Ki67-positive cells were counted manually within three high power fields (HPF) per sample in all probes 15 vs. 8 probes included in the study and then average was calculated (HPF: 40× objective lens).

Immunofluorescence staining (tissue): For immunofluorescent stainings, 2-µm sections were mounted on 0.1% poly-L-lysine (Sigma-Aldrich, St. Louis, MO, USA) pre-coated SuperFrost Plus slides (Thermo Fisher Scientific, Waltham, MA, USA). For antigen retrieval, the slides were boiled in a pressure cooker with 10 nM citrate buffer (distilled water with citric acid monohydrate, pH 6.0) and endogenous peroxidase activity was blocked with 3% hydrogen peroxide. Two antibodies were applied after one another. For each antibody, samples were blocked for 1 h (5% horse serum, 1%BSA, 0,5% Triton-X100) and incubated with primary antibodies diluted in 5% horse serum overnight (ApoE 1:600 ab52607 and SMA 1:200 ab7817, both abcam). The appropriate secondary antibody was added for 1 h (in 5% horse serum) on the next day (Alexa488 goat anti-mouse 1:400 A11001 and Alexa647 goat anti-rabbit 1:400 A21245, both Thermo Fisher). Autofluorescence quenching and counter-staining with DAPI were performed. There were appropriate positive and negative controls for every target antibody. Images were acquired with a Zeiss Axioscan7 Scanner, using ZEN 3.3 software (Carl Zeiss Microscopy GmbH, Jena, Germany). In total,

4–6 patient samples were stained and the most representative ones were chosen for the composite figures.

**Immunofluorescent staining (cells):** Cells were seeded in 4-well chamber CultureSlides (REF354104, Falcon, Miami, FL, USA) and fixed with 4% PFA for 15 min. Then, permeabilization (1% saponin) and blocking (5% BSA, 0.3% Triton X-100) were performed. After that, cells were incubated with primary antibodies diluted in 3% goat serum + 0.3% Triton X-100 overnight (SM22 1:200 ab14106 and SMA 1:300 ab5691, both abcam). The appropriate secondary antibody was added for 1 h (3% goat serum + 0.3% Triton X-100) the next day (Alexa488 goat anti-rabbit 1:400 A11034, Thermo Fisher). Then, Phalloidin staining was performed: Phalloidin (1:80 A22287, Thermo Fisher) was diluted in 1% BSA + 0.3 % Triton X-100 and incubated for 30 min before counterstaining with DAPI. Appropriate negative controls were performed for every target antibody. Images were acquired with a Leica THUNDER Imager using LAS X software (Leica Microsystems, Germany) and Fiji Image J.

**RNA isolation and qPCR (tissue):** Tissues were cut in ~50 mg (approx.  $3 \times 3 \times 3$  mm) pieces with a scalpel on dry ice using a micro scale. Tissue was homogenized in 700  $\mu$ L Qiazol lysis reagent and total RNA was isolated using the miRNeasy Mini Kit (Qiagen, Venlo, The Netherlands) according to manufacturer's instruction. RNA concentration and purity were assessed using the NanoDrop. Next, first strand cDNA synthesis was performed using the High-Capacity-RNA-to-cDNA Kit (Applied Biosystems, Waltham, MA, USA), following the manufacturer's instruction.

Quantitative real-time TaqMan PCR was then performed using Taqman Gene Expression Master Mix (Thermo Fisher, Darmstadt, Germany). PCR was run on a QuantStudio3 Cycler (Applied Biosystems, Waltham, MA, USA) using 96 well plates. Gene expression was normalized to Rplp0 and quantified with the  $2^{\Delta\Delta Ct}$  method.

Primer list: APOE (Hs00171168\_m1), LDLR (Hs01092524\_m1), LRP1 (Hs00233856\_m1), ABCA1 (Hs01059101\_m1), ABCG1 (Hs00245154\_m1), MMP9 (NM 004994.2), MYH11 (NM 002474.2); ACTB (NM\_001101); MMP9 (NM 004994.2); MYH11 (NM 002474.2)

**Affymetrix mRNA expression profile analysis:** RNAs from aneurysm and control tissue samples were reverse transcribed, labeled and hybridized to Affymetrix PrimeView (Thermo Fisher, Germany) gene expression microarrays according to the manufacturer's instructions. Data analysis was performed in R with Bioconductor packages. Briefly, data were read with package affy, normalization was performed with package vsn and differentially expressed genes were defined with package limma [26]. The raw data are shown in Table S3.

**Cell treatment, RNA isolation and qPCR (Primary PAA cells/human aortic SMCs):** Cells were placed in 12-well plates (triplicates each) and treated with 50  $\mu$ g/mL ApoE (ab280330, Abcam, Cambridge, UK) in OptiMEM +2% FBS (Thermo Fisher, Dreieich, Germany) or OptiMEM +2%FBS only (control-treatment) for 6 h, 24 h, 48 h and 72 h. Cells were washed with PBS and harvested with 300  $\mu$ L Qiazol lysis reagent. Total RNA was isolated using the RNeasy Mini Kit (Qiagen, Venlo, The Netherlands) according to manufacturer's instruction. RNA concentration and purity was assessed using the NanoDrop. Next, first strand cDNA synthesis was performed using the High-Capacity-RNA-to-cDNA Kit (Applied Biosystems, USA), following the manufacturer's instruction.

Quantitative real-time TaqMan PCR was then performed using Taqman Gene Expression Master Mix (Thermo Fisher, Germany). PCR was run on a QuantStudio3 Cycler (Applied Biosystems, USA) using 96-well plates. Gene expression was normalized to Rplp0 and quantified with the  $2^{\Delta\Delta Ct}$  method.

Primer list: RPLP0 (Hs00420895\_gH), MYOCD (Hs00538076\_m1), TAGLN (Hs0103877\_7\_g1), ACTA2 (Hs00426835\_G1), SMTN (Hs01022255\_g1), CNN1 (Hs00959434\_m1), KLF4 (Hs00358836\_M1), CD34 (Hs02576480\_m1), CD44 (Hs01075864\_m1), VIM (Hs00958111\_m1), COL1A1 (Hs00164004\_M1).

**WESTERN BLOT:** Cells were placed in 6-well plates (triplicates each) and treated with 50  $\mu$ g/mL ApoE in OptiMEM (Thermo Fisher, USA, Lenvatinib-treatment) or OptiMEM (control-treatment) for 48 h. Cells were washed with ice-cold PBS and harvested with 100  $\mu$ L

freshly prepared complete RIPA Buffer (RIPA Lysis and Extraction Buffer, Thermo Fisher, Waltham, MA, USA) containing Phosphatase Inhibitor Cocktail 2 and 3 (Sigma Aldrich, St. Louis, MO, USA) and Halt™ Protease Inhibitor Cocktail (Thermo Fisher, USA). After homogenization with a pistil lysate was frozen at  $-80^{\circ}\text{C}$  in aliquots of total protein lysate.

Following the manufacturer's instruction, total protein concentration was measured using the Pierce™ BCA Protein Assay Kit (Thermo Fisher, USA).

An amount of 10  $\mu\text{g}$  of protein of each sample was denatured and reduced at  $95^{\circ}\text{C}$  for 10 min, then separated in a Bolt™ 4–12% Bis-Tris Plus Gel (Thermo Fisher, USA) and transferred onto Trans-Blot® Turbo™ Transfer Pack Membranes (BioRad, Hercules, CA, USA). The blots were blocked with 5% BSA in Tris-buffered saline + 0.1% Tween-20 for 1 h, followed by overnight incubation with the primary antibody against SMTN (ab8969, Abcam, UK), CNN1 (ab46794, Abcam, UK), and SM22 (ab14106, Abcam, UK) in TBS-T + 5% BSA. After washing with TBS-T, blots were then incubated with anti-mouse- or anti-rabbit-HRP (horseradish peroxidase)-conjugated secondary antibodies (ab205718, ab205719, Abcam, UK) and visualized using ECL Prime Western Blotting Detection Reagent (Amersham, Amersham plc, UK) in the C600 Azure Biosystems Imager 585 (Biozym) / ChemiDoc XRS System (Bio-rad, Hercules, CA, USA). Blots were stripped using Restore™ Plus Western Blot Stripping Buffer (Thermo Fisher, USA), blocked again with 5% BSA in TBS-T and incubated with the primary antibody against  $\beta$ -Actin (A1978-200  $\mu\text{L}$ , Sigma Aldrich, USA) in TBS-T + 5% BSA for 1 h. After washing with TBS-T, blots were again incubated with anti-mouse-HRP (horseradish peroxidase)-conjugated secondary antibody (ab205719, Abcam, UK) and visualized using ECL Prime Western Blotting Detection Reagent (Amersham, Amersham plc, UK) in the C600 Azure Biosystems Imager 585 (Biozym) / ChemiDoc XRS System (BioRad, Hercules, CA, USA). Antibodies and dilutions: SMTN, ab8969: 1:1000; CNN1, ab46794: 1:5000; SM22, ab14106: 1:1000,  $\beta$ -Actin, A1978: 1:8000; Goat-Anti-Rabbit IgG H&L HRP, ab205718: 1:10,000; Goat-Anti-Mouse IgG H&L HRP, ab205719: 1:10,000.

The blots were quantitated by using Fiji ImageJ Software. (Complete membranes/gels are shown in Figure S5).

**Dynamic live-cell imaging assay:** Dynamic live-cell imaging experiments were performed following the instructions provided by Essen Bioscience (Ann Arbor, MI, USA) using the IncuCyte ZOOM system.

**Proliferation:** Cells were placed with 30% confluence in a 96-well plate and treated with 50  $\mu\text{g}/\text{mL}$ , 5  $\mu\text{g}/\text{mL}$  and 0.5  $\mu\text{g}/\text{mL}$  ApoE (ab280330, Abcam, UK) in OptiMEM +2% FBS (Thermo Fisher, Germany) or OptiMEM +2% FBS only (control-treatment) for 72 h. The plate was monitored in the IncuCyte ZOOM System (Essen Bioscience, Ann Arbor, MI, USA) with phase contrast and a 2 h imaging pattern. Images were auto-collected and analyzed using the IncuCyte ZOOM software (Essen Bioscience, Ann Arbor, MI, USA) and GraphPad Prism 9.4.1.

**Migration:** Cells were placed with 100% confluence in a 96-well ImageLock™ plate (Essen Bioscience, Ann Arbor, MI, USA). A wound was created using the Incucyte® 96-Well Woundmaker Tool (Essen Bioscience, Ann Arbor, MI, USA), according to the manufacturer's instructions. After 2 washes with PBS, the cells were treated with 50  $\mu\text{g}/\text{mL}$ , 5  $\mu\text{g}/\text{mL}$  and 0.5  $\mu\text{g}/\text{mL}$  ApoE (ab280330, Abcam, UK) in OptiMEM +2% FBS (Thermo Fisher, Germany) or OptiMEM +2% FBS only (control-treatment) for 72 h. The plate was monitored in the IncuCyte ZOOM System (Essen Bioscience, Ann Arbor, MI, USA) with phase contrast and a 1 h imaging pattern. Images were auto-collected and analyzed using the IncuCyte ZOOM software (Essen Bioscience, Ann Arbor, MI, USA) and GraphPad Prism 9.4.1.

**OLink Protein analysis:** For potential proteomic target identification, we used the commercially available OLink® high-throughput, multiplex immunoassay according to the manufacturer's protocol. Briefly, protein lysates were generated from whole vessel wall samples of 6 non-aneurysmatic popliteal arteries (PA), 16 PAA and 19 AAA samples using Laemmli buffer (normal popliteal arteries were from the same patients as PAAs). Afterwards, 1  $\mu\text{L}$  of undiluted protein was sent to the company (OLink) as requested by the protocol and the cardiovascular panels CVD II and CVD III were used to screen for a

total of 180 cardiovascular proteins by Proseek® Multiplex—Proximity Extension Assay. Four proteins served as internal validation control in both panels. Afterward, Proseek generates Cq values, and these were normalized by extension control ( $dCq_{analyte} = Cq_{analyte} - Cq_{Ext\ Ctrl}$ ), interpolate control ( $ddCq = dCq_{analyte} - dCq_{Interpolate\ Ctrl}$ ) and normalization against a calculated correction factor ( $NPX = \text{Correction factor} - ddCq$ ). Finally, Normalized Protein eXpression (NPX) values are given as Log 2 scale (high NPX value = high protein concentration) as described before [27,28].

Comparative analysis of Affymetrix gene expression and Olink protein quantification data with pathway enrichment analysis: Expression was further analyzed for pathway enrichment through Gene Set Enrichment Analysis (GSEA), using GSEA version 4.3.2 together with KEGG and Molecular Signatures Database Hallmarks gene sets (Supplement Table S4) [29–32]. A gene-wise ranking score using  $\log FC / \text{abs}(\log FC) \times -\log 10(p\text{-value})$  from differential expression results was used to combine significance and direction of change. These scores were used to run GSEA pre-ranked KEGG and Hallmark enrichment analysis with a minimum gene set size of 5. Noteworthy enrichments were considered when categories reached a nominal  $p\text{-value} < 0.05$  in at least one comparison.

Case report mechanical PAA: Tissue from the “mechanical PAA” was obtained from a 51-year-old male former soldier with a smoking history. Upon occasional swelling and pain in the left knee, especially after exercising, he was diagnosed with an aneurysmatic lesion and an osseous lesion at the back of the tibia directly adjacent to the popliteal artery in MRA and X-ray (Figure S1A). A previous trauma or surgery was not reported. The aneurysm was excised and a venous bypass graft was implanted. The osseous lesion was carefully removed. The patient was dismissed after 5 days in good condition and has been symptom-free. The contralateral leg showed no similar pathology.

Statistics: Comparison of Ki67 positive cell turnover was performed by cell counting per high power field and analysis with the Mann–Whitney test. Graphs and figures were created with Excel®, PowerPoint® (Microsoft) (Office Professional Plus 2016) and R (<http://www.r-project.org/>, accessed on 21 June 2023). Expression values were compared using the Mann–Whitney test with the level of significance at 0.05. Gene Expression Results were analyzed using GraphPad Prism 9.4.1 and student’s *t*-test.

### 3. Results

VSMC phenotype switch and comparison to AAA:

PAA vessel wall samples showed a distinct histomorphology with loss of the typical muscular-type artery architecture including the internal and external elastic lamina in comparison to non-aneurysmatic PA from the same patient (Figures 1A and S1A). Ki67 staining reveals a highly significant increased number of proliferating cells within the aneurysmatic vessel wall (Figure 1B). Vimentin and  $\alpha$  smooth muscle actin (SMA) positive vascular smooth muscle cells (VSMC) show a loss of desmin as part of the contractile apparatus (Figures 1C and S1A). This VSMC phenotype switch from contractile senescent to proliferating dedifferentiated is also a feature of AAA in comparison to non-aneurysmatic aortic wall previously described by others and us [16,33].

Additional features of AAA, such as upregulation of genes involved in the vascular endothelial growth factor (VEGF) receptor and the transforming growth factor  $\beta$  (TGF $\beta$ ) receptor signaling pathways, are found similarly in PAA as compared to non-aneurysmatic arteries (Figures 1D and S1B). Moreover, MMP 9 was found to be significantly upregulated in PAA, whereas pro-apoptotic B-cell lymphoma 2 (BCL2) was found upregulated in AAA but unchanged in PAA D and Figure S1B). Of note, inflammatory genes tended to be less upregulated in PAA as in AAA (Figure S1B).

Immunohistochemistry and expression analysis revealed no such results in a singular case of PAA caused by osseous mechanical strain (case description s. above). Here, the lamellar histomorphology was preserved, desmin was still present in VSMCs and dilated and non-dilated tissue sections were hierarchically clustered with non-aneurysmatic arteries upon expression profiling (Figure S1A,C).

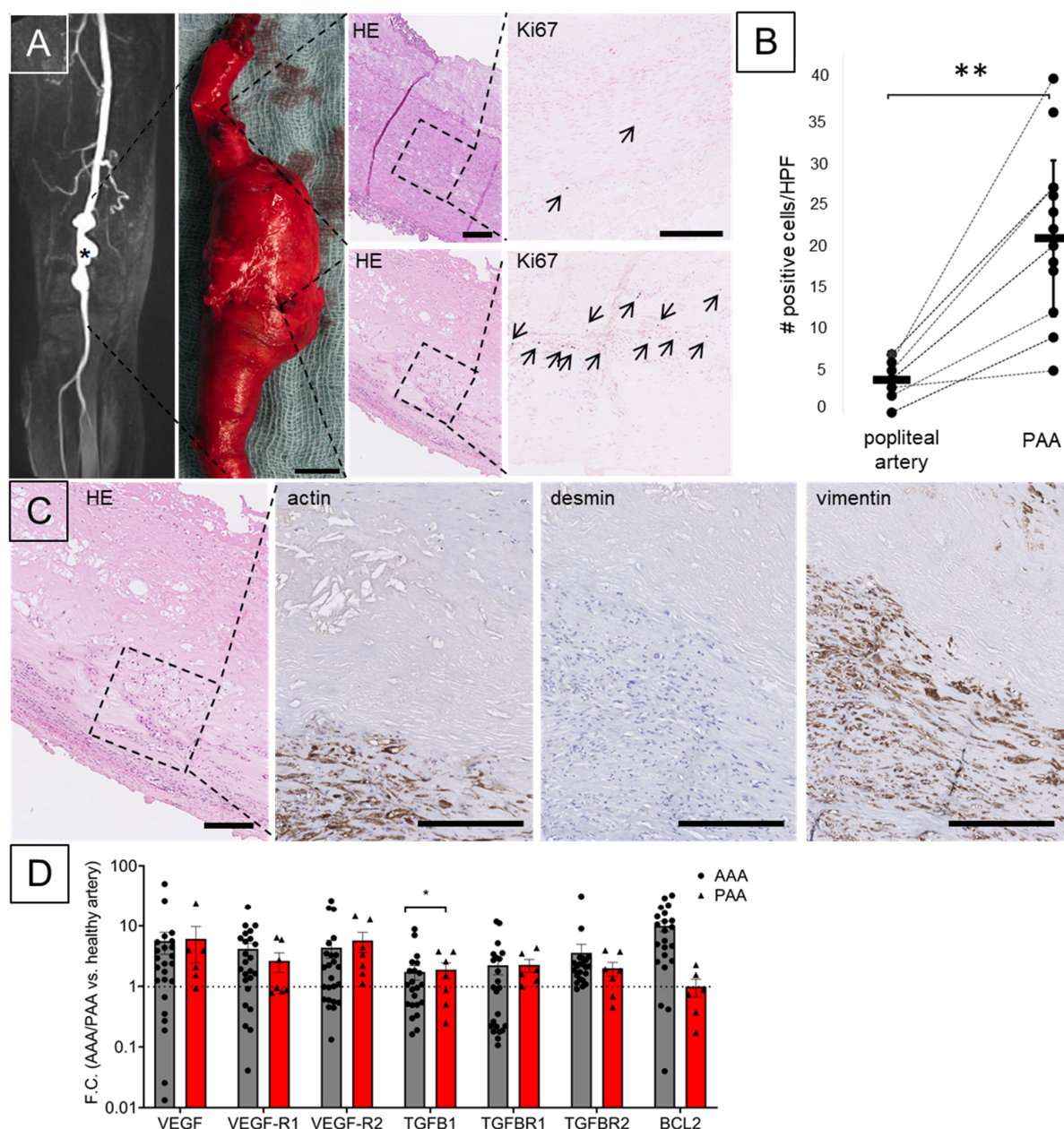


**Figure 1.** PAA immunohistochemistry, cell proliferation and qPCR results. (A) PAA morphology is characterized by vessel dilation (\*) on MR-angiography and after surgical resection (scale bar 10 mm). Histological analysis of PAA compared to normal popliteal artery shows calcifications, destruction of elastic fibers, collagen enrichment and angiogenesis on hematoxylin/eosin (HE) staining. (B) Ki67 staining (arrow in (A)) and cell counting revealed a significant number of proliferating cells in PAA compared to non-aneurysmatic arteries. (C) PAA tissue shows loss of the VSMC contractile marker desmin compared to actin and vimentin (non-aneurysmatic popliteal artery: Figure S1A) (scale bar: 100  $\mu$ m). (D) Gene Expression Analysis of PAA (red) and AAA (grey) shown as fold change vs. the respective non-aneurysmatic vessel (AAA vs. aorta:  $n = 24$  vs.  $n = 10$ ; PAA vs. popliteal artery:  $n = 7$  vs.  $n = 8$ ; PAA vs. AAA: unpaired  $t$ -test, \*  $p < 0.05$ , \*\*  $p < 0.01$ ).

Gene array analysis, expression of apolipoprotein E (ApoE) and pathway enrichment:

An exploratory Affymetrix© array identified genes of the VSMC contractile apparatus down- and MMPs to be dysregulated in PAA compared to PA (Figures 2A and S1C, Tables S2 and S3). Genes from the apolipoprotein E/C1 locus were also dysregulated. Utilizing qPCR, *APOE* expression in PAA compared to PA was not significant in this small

cohort ( $p = 0.1$ ) (Figure 2C). Similar trends were observed for AAA ( $p = 0.11$ ) and PAOD samples ( $p = 0.41$ ) (Figure 2D).

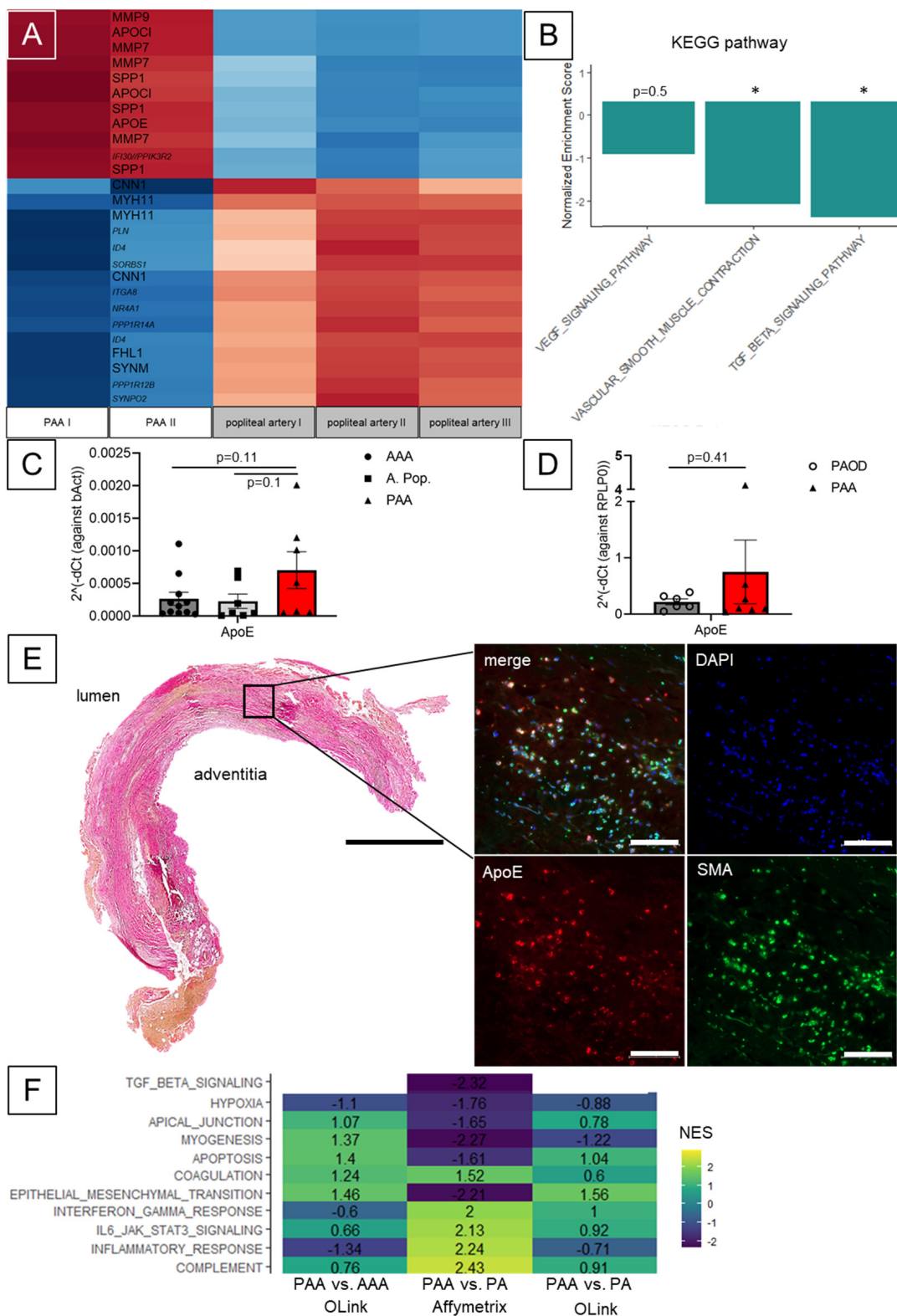


**Figure 2.** Affymetrix Analysis, Pathway enrichment, comparative ApoE expression and PAA immunofluorescence. (A) Gene expression heatmap (top 25 hits, cutout from Figure S1C) with hierarchical clustering for PAA vs. popliteal artery based on lowest adjusted  $p$ -value (all  $> 0.05$ : Supplement

Table S3) (annotations: Table S2). (B) Selected examples of KEGG pathway enrichment based on Affymetrix data (NES: normalized score shown in (F), \* =  $p < 0.05$ ). (C) RT-qPCR results of ApoE expression in PAA (red) compared to popliteal artery (light grey), AAA (dark grey) and (D) PAOD (grey) shown as  $2^{\Delta\Delta Ct}$  values against the respective housekeeping gene ( $n = 11$  AAA,  $n = 7$  A. pop.,  $n = 7$  PAA;  $n = 6$  PAOD,  $n = 7$  PAA; mean +/- SEM; unpaired  $t$ -test, \*  $p < 0.05$ ). (E) PAA tissue sample (HE; scale bar 2 mm) and immunofluorescence with APOE (red) and SMA (green)-positive cells co-localization (scale bar 100  $\mu$ m). (F) Exemplary comparative hallmarks pathway enrichment analysis of Affymetrix gene expression data and OLink Protein expression data for PAA vs. popliteal artery (PA) and PAA vs. AAA (all  $p$ -value < 0.05) (complete enrichment sets shown in Figure S4).

Despite this non-significant gene expression analysis, on the cellular level, APOE co-localized with SMA-positive cells upon immunofluorescence in the media of PAA samples (Figures 2E and S2C). Of note, CD-68 positive cells were seen abundantly in PAA samples, too (Figure S2A). Genes involved in cholesterol homeostasis, e.g., phospholipid-transporting ATPase (ABCA1), were found to be higher expressed in PAA tissue compared PAOD plaque samples ( $p = 0.03$ ) (Figure S3A).

Accordingly, a KEGG pathway and hallmarks enrichment analysis of the PAA vs. non-aneurysmatic artery gene expression data identified VSMC contraction (NES -2.2;  $p < 0.05$ ) and TGF $\beta$  signaling (-2.4;  $p < 0.05$ ) to be negatively correlated with PAA (Figures 2B and S4). VEGF (-1.1;  $p = 0.5$ ) and Apoptosis (ES 1.0;  $p = 0.6$ ) enrichments were not significant.

Additionally, data from a separate proteomic approach (OLink) with PAA, PA and AAA tissue lysates allowed comparative enrichment analysis (Figure S4). Here, comparison of genetic (PAA vs. PA only) and proteomic (PAA vs. PA and PAA vs. AAA) data revealed negative enrichment of APOPTOSIS (Hallmark) at genetic levels, yet positive enrichment at proteomic levels, similar to PAA and AAA (Figures 2F and S4, Tables S3 and S4).

APOE decreases cell growth in primary human cell culture by VSMC phenotype restoration:

To test a possible effect of ApoE on VSMCs, a primary human PAA cell culture was established. Here, the expression of VSMC markers, such as SMA (ACTA2) or SM22 (TAGLN) positivity and a typical SMC shape (indicated by phalloidin staining) was observed in accordance to established and commercially available primary human aortic (hAo)SMCs (Figures 3A and S2B). Live cell imaging revealed a dose- and time-dependent inhibitory effect on the proliferation over 72 h in both primary human cell cultures (Figure 3B). Here, 50  $\mu$ g/mL ApoE significantly decreased the cell proliferation rate (indicated by less confluence) from 48 h onwards compared to untreated cells. No effect on cell migration was observed (Figure S4D). Of note, hAoSMCs showed an earlier and more pronounced response than primary human PAA-derived cells.

A VSMC phenotype marker gene expression panel at different time points revealed significant upregulation of myocardin 1 (MYOCD) or smoothelin (SMTN) upon APOE treatment PAA VSMCs after 48 h (Figures 3C and S3B). Again, MYOCD upregulation was seen already at 6 h in hAoSMCs (Figures 3D and S3C). Additionally, WB analysis revealed higher abundance of calponin1 in PAA and aortic SMCs after ApoE stimulation for 48 h and similar trends for smoothelin and SM22 (Figures 3E and S3D). However, quantitative analysis normalized to  $\beta$ -actin was not significant.

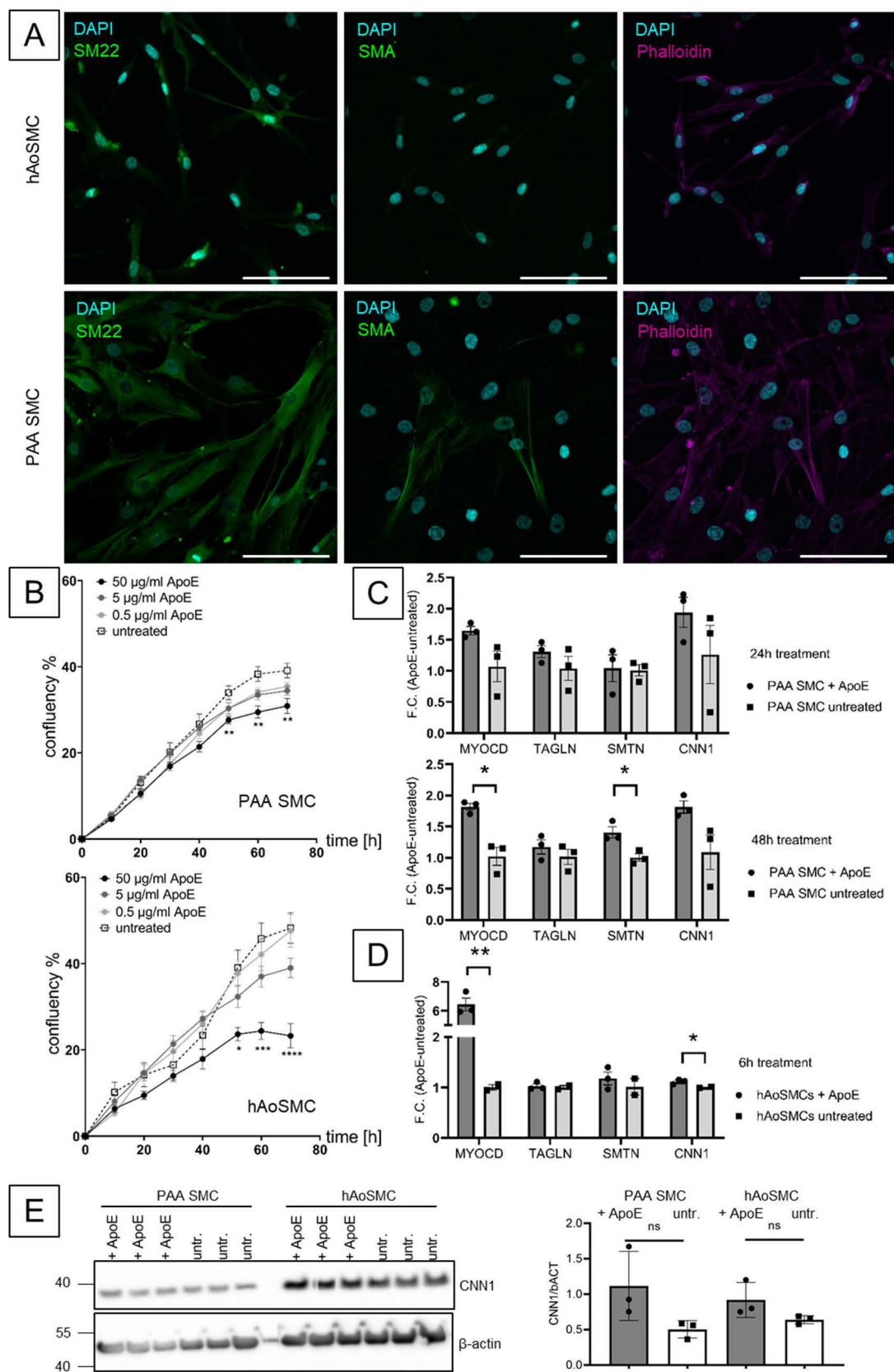


**Figure 3.** PAA primary cell culture immunofluorescence, Incucyte<sup>©</sup> live cell imaging and contractile VSMC marker genes analysis. (A) PAA cells show similar morphology and expression of SMC-specific markers (SM22, SMA) and overall morphology (phalloidin) when compared to AoSMCs (scale bar

100  $\mu$ m). (B) Live cell imaging depicts changes in confluence over time with different ApoE treatment concentrations for human aortic smooth muscle cells (left) and primary PAA patient-derived cells (two-way ANOVA treated vs. untreated, \*  $p < 0.05$ , \*\*  $p < 0.01$ , \*\*\*  $p < 0.001$ , \*\*\*\*  $p < 0.0001$ ; Mean +/− SEM). (C) Exemplary RT-qPCR results of VSMC contractile marker gene expression at 24 h and 48 h after ApoE treatment (dark grey vs. no treatment light grey) for PAA primary cells and (D) at 6 h for human aortic SMCs (both 50  $\mu$ g/mL ApoE) (unpaired *t*-test) (full panel in Figure S3B,C). (E) WB and quantification for CNN1 normalized to  $\beta$ -actin for PAA SMCs and hAoSMCs upon ApoE stimulation.

#### 4. Discussion

This study suggests that PAA might have a distinct pathophysiology compared to AAA, PAOD and sole mechanic strain, despite sharing some common pathway involvements. Specifically, APOE overrepresentation in tissues, demonstrated on gene and protein levels for the first time, might be involved in the VSMC phenotype switch and possible restoration of the contractile phenotype (Figure 4). Here, no significant dysregulations in lipid metabolism-associated pathways were identified, emphasizing a potential additional function of APOE for individual patients.

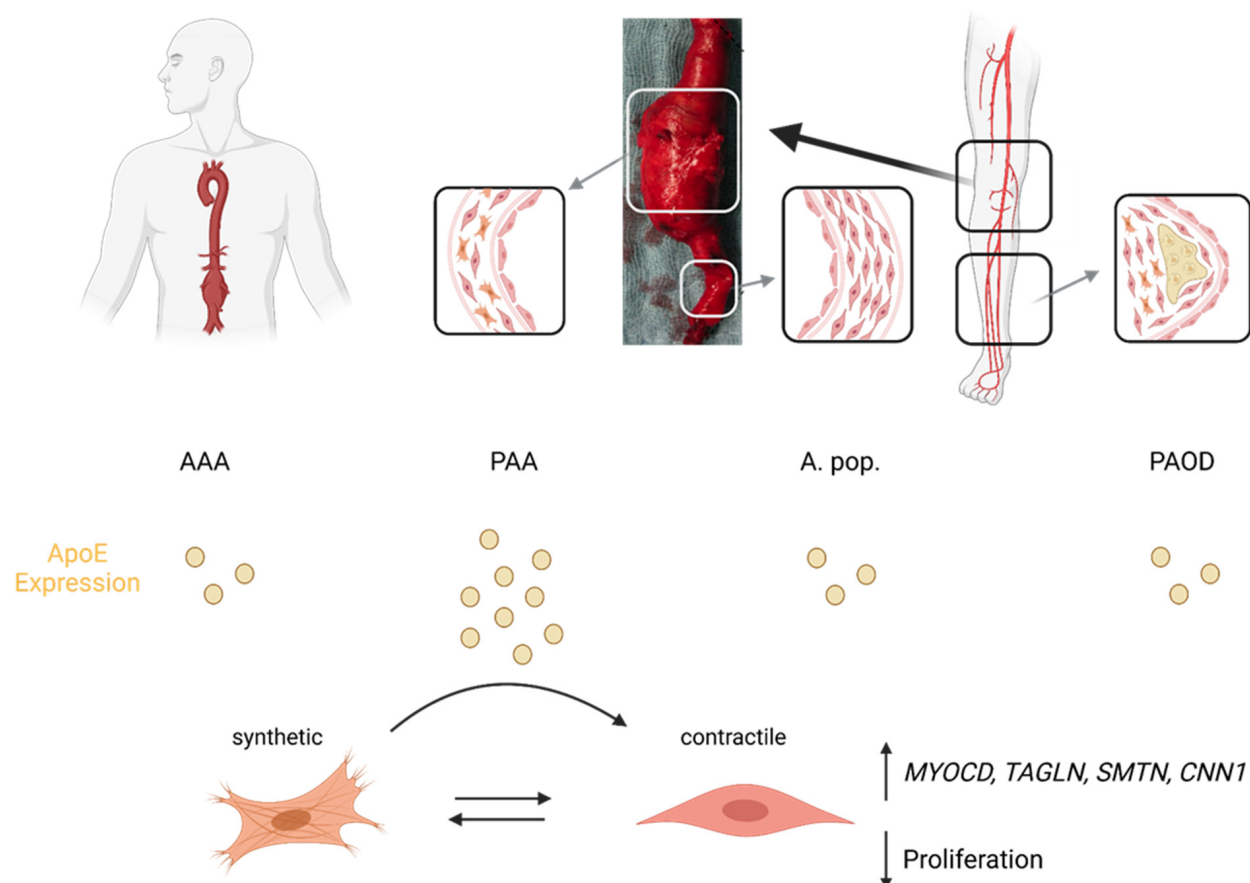


**Figure 4.** Illustrated abstract. Schematic depiction of proposed speculative mechanism (created with BioRender.com). ApoE is more abundant in tissues from PAA patients compared to non-dilated A. pop. or other vascular diseases (AAA and PAOD). Treatment of VSMCs with ApoE leads to decreased proliferation and increased expression of contractile markers such as MYOCD, TAGLN, SMTN and CNN1on RNA and protein levels. Overall, this study suggest that ApoE might be involved in contractile phenotype restoration of popliteal VSMCs and thus counteract aneurysm formation (in individual patients).

However, disease heterogeneity might be high among PAA patients on histomorphologic and molecular level as reported for AAA patients, possibly in accordance with

individual aneurysm diameter [16,34]. Individually, PAA growth and eventual intraluminal thrombus (ILT) formation might be mechanically driven, while others have a distinct pathomechanism [35]. Recently, a microRNA (miRNA) and circulating MMP signature for popliteal involvement have been identified in patients with multiple aneurysm sites [23,36–38]. Here, we demonstrate similar involvement of VSMC phenotype switch, VEGF and TGF $\beta$  signaling and change in histomorphology in PAA as compared to AAA (Figures 1, 2A and S1B). Additionally, based on a singular case with possible isolated osseous strain on the popliteal artery, so-called Nora’s lesion, we demonstrate a preserved VSMC phenotype and expression profile in this patient (Figure S1) [10,11,39]. Generally, a modest inflammatory component is described for PAA samples. However, more inflammatory subtypes, as also known for AAA, have been reported [16,23,40,41]. No increased expression of inflammatory genes was observed (Figure S1B).

Unique in this study, *APOE* was found more abundant in PAA tissue in comparison to PA and AAA (Figure 2C,D). *APOE* has been shown to play a detrimental role in atherosclerosis and vascular research—and *ApoE*<sup>−/−</sup> mice are the most frequently used pro-atherosclerotic animal model for various vascular diseases [42]. However, depending on the genetic risk alleles for *APOE*, its role differs among patients [43]. Here, we demonstrate a general up(dys-)regulation, yet with mentionable variance (Figure 2A,C). Hence, the individual role in PAA pathogenesis might differ between individuals.

Generally, *APOE* is involved in cholesterol hemostasis functioning as lipoprotein. Aneurysm and atherosclerotic diseases share many common features, such as matrix remodeling, macrophage homing and calcification. Atherosclerosis to a greater or minor extent is observed in almost every AAA patient. The associated diseases such as coronary artery disease and carotid artery disease, as well as PAOD, are observed more frequently in this cohort [44,45]. However, the onset of disease might differ. Atherosclerosis is considered a disease of the intima, since the early stages of the disease are seen here [46]. AAA is considered a disease of the media based on the early changes observed in animal models [47,48]. The specific role of mechanisms identified in both entities might also differ due to different susceptibility of the vessel wall to the same stimuli such as TGF $\beta$  signaling, early in embryogenesis and later in adulthood [49,50]. Here, we show that *APOE* is more abundant in PAA tissues in comparison to AAA and PAOD (Figure 2B). In addition, genes, known to be upregulated in AAA samples are also found upregulated in PAA and the exploratory proteomic-based pathway enrichment analysis demonstrates similarities of both diseases (Figures 2F and S4). However, further research needs to validate common features and distinct differences between AAA, PAA and atherosclerosis. Moreover, the subcellular mechanistic insights on VSMC phenotype switch of *ApoE* warrant further elucidation. Most available studies only provide indirect data using *apoE*<sup>−/−</sup> mice for mechanistic investigations [51,52].

VSMC phenotype switch is observed in both, aneurysm and atherosclerosis; however, probably to a different extent and with heterogeneous clonality [24,52,53]. Others have reported increased apoptosis by p53 upregulation and loss of VSMCs in PAA samples [54,55]. This aligns with previous reports from AAA, where VSMC loss in matrix remodeling is frequently discussed [23,56]. However, these results must be discussed carefully, since the VSMC phenotype switch might lead to different staining properties. Generally, ECM deposition and vessel wall thickening might be misinterpreted as cellular content loss [47]. VSMC density is still high in PAA samples and cell turnover seems to be high (Figures 1B and 2E). VSMC phenotype switch as a target for aneurysm growth alteration has been successfully demonstrated by us and others [18,57]. Additionally, other target genes, not previously involved in aneurysm research, however, also found to be dysregulated in our samples might be worthwhile investigating in future research, e.g., for their role in specific pathways (Figures 1A and S4B,C, Table S2).

Limitations of the study are the relatively low numbers of patients and samples included, as well as the only exploratory character of gene expression and proteomic analysis. Hence, conclusions can only be drawn lacking statistical significance and remain

speculative. So far, no relevant animal models for PAA have been reported [42]. Regarding the successful implementation of a primary human cell culture in this study, organ-on-a-chip or organoids could be helpful for further research (Figure 3) [58]. However, control cells from human non-dilated “healthy” popliteal artery, currently not available from surgical sites, should be included. Owing to its peripheral localization and the reasonably easy access by endovascular means, local medical, i.e., drug-coated balloon treatment, could be a desirable translational aspect [7,18]. Whether APOE, APOE-modifying chemicals or completely different substances are the most promising targets warrants further research.

## 5. Conclusions

In conclusion, APOE was found to be dysregulated in PAA samples compared to non-aneurysmatic popliteal arteries, AAA and PAOD human tissue samples and co-localized with VSMCs demonstrated to switch their phenotype. APOE stimulation of primary human aortic and popliteal VSMCs reduced cell proliferation and increased contractile cellular marker gene and protein expression. Further research needs to validate these preliminary findings and elucidate future translational applications.

**Supplementary Materials:** The following supporting information can be downloaded at: <https://www.mdpi.com/article/10.3390/biom13071074/s1>. Figure S1: False aneurysm case presentation, histologic analysis, qPCR results from comparative analysis and gene expression heatmap. Figure S2: PAA immunohistochemistry and fluorescence imaging negative controls. Figure S3: Cholesterol hemostasis gene panel and primary cell gene expression results. Figure S4: Comparative pathway enrichment analysis. Figure S5: WB full membranes. Table S1: Detailed patients’ characteristics. Table S2: Annotations of the significant genes in PAA vs. popliteal artery gene expression analysis from Figure 2A. Table S3: Excel file with Affymetrix results. Table S4: Excel file with OLink results.

**Author Contributions:** Conceptualization, A.B. and L.M.; Methodology, J.P., T.R., N.S., E.C., C.O., C.-J.S. and A.B.; Software, C.-J.S.; Validation, G.W., N.S., H.F., C.R., H.-H.E. and A.B.; Formal Analysis, J.P. and A.B.; Resources, L.M., A.B., H.-H.E., C.R. and C.O.; Data Curation, G.W. and C.-J.S.; Writing—Original Draft Preparation, A.B. and J.P.; Writing—Review and Editing, all authors; Visualization, J.P. and C.-J.S.; Supervision, L.M. and A.B.; Funding Acquisition, C.O., L.M. and A.B. All authors have read and agreed to the published version of the manuscript.

**Funding:** The study was funded by the Interdisciplinary Center for Clinical Research (IZKF) Würzburg (Z3\_25) and a grant given to AB by the German Vascular Society (DGG). AB was granted a Research Fellowship by the German Research Foundation (DFG). CJS was funded by the IZKF Würzburg (Z-6). LM received funding from the European Research Council (ERC-CoG project LongTx under the grant agreement number 101088370), a DZHK Translational Research Project (TRP), the SFB1123 and TRR267 of the German Research Council (DFG), as well as Vetenskapsrådet (2019-01577), and Hjärt-Lungfonden (20210450).

**Institutional Review Board Statement:** Tissue acquisition was in accordance with the declaration of Helsinki, with approval of the local ethic review committee (University of Würzburg 20181107\_02; Technical University Munich: 2799/10) and with patients’ informed and written consent.

**Informed Consent Statement:** Informed consent for biobank inclusion was collected from all patients involved.

**Data Availability Statement:** Not applicable.

**Acknowledgments:** We are very thankful to M. Koopal, M. Hofmann, B. Mühling, M. Göbel, C. Pregitzer and N. Glukha for their most skillful technical assistance. B. Davoudi and S. Bauer helped with slide scanning. Mariette Lengquist gratefully performed a pilot  $\alpha$ SMactin/Ki67 double staining.

**Conflicts of Interest:** LM is a scientific consultant and adviser for Novo Nordisk (Malov, Denmark), DrugFarm (Shanghai, China) and Angiolutions (Hannover, Germany), and received research funds from Roche Diagnostics (Rotkreuz, Switzerland) and Novo Nordisk (Malov, Denmark). Albert Busch is a consult for Angiolutions (Hannover, Germany) and Brainlab (Munich, Germany). All other authors report no conflicts of interest.

## References

- Trickett, J.; Scott, R.; Tilney, H. Screening and management of asymptomatic popliteal aneurysms. *J. Med. Screen.* **2002**, *9*, 92–93. [[CrossRef](#)] [[PubMed](#)]
- Tuveson, V.; Löfdahl, H.E.; Hultgren, R. Patients with abdominal aortic aneurysm have a high prevalence of popliteal artery aneurysms. *Vasc. Med.* **2016**, *21*, 369–375. [[CrossRef](#)] [[PubMed](#)]
- Ravn, H.; Wanhainen, A.; Björck, M. Risk of new aneurysms after surgery for popliteal artery aneurysm. *Br. J. Surg.* **2008**, *95*, 571–575. [[CrossRef](#)] [[PubMed](#)]
- Cross, J.; Galland, R. Part One: For the Motion: Asymptomatic Popliteal Artery Aneurysms (less than 3 cm) Should be Treated Conservatively. *Eur. J. Vasc. Endovasc. Surg.* **2011**, *41*, 445–448; discussion 449. [[CrossRef](#)]
- Naazie, I.N.; Arbabi, C.; Moacdieh, M.P.; Hughes, K.; Harris, L.; Malas, M.B. Female sex portends increased risk of major amputation following surgical repair of symptomatic popliteal artery aneurysms. *J. Vasc. Surg.* **2022**, *76*, 1030–1036. [[CrossRef](#)] [[PubMed](#)]
- Grip, O.; Mani, K.; Altreuther, M.; Gonçalves, F.B.; Beiles, B.; Cassar, K.; Davidovic, L.; Eldrup, N.; Lattmann, T.; Laxdal, E.; et al. Contemporary Treatment of Popliteal Artery Aneurysms in 14 Countries: A Vascunet Report. *Eur. J. Vasc. Endovasc. Surg.* **2020**, *60*, 721–729. [[CrossRef](#)]
- Cervin, A.; Tjärnström, J.; Ravn, H.; Acosta, S.; Hultgren, R.; Welander, M.; Björck, M. Treatment of Popliteal Aneurysm by Open and Endovascular Surgery: A Contemporary Study of 592 Procedures in Sweden. *Eur. J. Vasc. Endovasc. Surg.* **2015**, *50*, 342–350. [[CrossRef](#)]
- Trinidad-Hernandez, M.; Ricotta, J.J., II; Gloviczki, P.; Kalra, M.; Oderich, G.S.; Duncan, A.A.; Bower, T.C. Results of elective and emergency endovascular repairs of popliteal artery aneurysms. *J. Vasc. Surg.* **2013**, *57*, 1299–1305. [[CrossRef](#)]
- Farber, A.; Angle, N.; Avgerinos, E.; Dubois, L.; Eslami, M.; Geraghty, P.; Haurani, M.; Jim, J.; Ketteler, E.; Pulli, R.; et al. The Society for Vascular Surgery clinical practice guidelines on popliteal artery aneurysms. *J. Vasc. Surg.* **2021**, *75*, 109S–120S. [[CrossRef](#)]
- Nasr, B.; Albert, B.; David, C.H.; da Fonseca, P.M.; Badra, A.; Gouny, P. Exostoses and Vascular Complications in the Lower Limbs: Two Case Reports and Review of the Literature. *Ann. Vasc. Surg.* **2015**, *29*, 1315.e7–1315.e14. [[CrossRef](#)] [[PubMed](#)]
- Nora, F.E.; Dahlin, D.C.; Beabout, J.W. Bizarre parosteal osteochondromatous proliferations of the hands and feet. *Am. J. Surg. Pathol.* **1983**, *7*, 245–250. [[CrossRef](#)]
- Stephenson, M.A.; Vlachakis, I.; Valenti, D. Bilateral popliteal artery aneurysms in a young man with Loeys-Dietz syndrome. *J. Vasc. Surg.* **2012**, *56*, 486–488. [[CrossRef](#)]
- Koksoy, C.; Gyedu, A.; Alacayir, I.; Bengisun, U.; Uncu, H.; Anadol, E. Surgical Treatment of Peripheral Aneurysms in Patients with Behcet's Disease. *Eur. J. Vasc. Endovasc. Surg.* **2011**, *42*, 525–530. [[CrossRef](#)]
- Debasso, R.; Astrand, H.; Bjarnegard, N.; Ryden Ahlgren, A.; Sandgren, T.; Lanne, T. The popliteal artery, an unusual muscular artery with wall properties similar to the aorta: Implications for susceptibility to aneurysm formation? *J. Vasc. Surg.* **2004**, *39*, 836–842. [[CrossRef](#)]
- De Basso, R.; Astrand, H.; Ahlgren, A.R.; Sandgren, T.; Lanne, T. Low wall stress in the popliteal artery: Other mechanisms responsible for the predilection of aneurysmal dilatation? *Vasc. Med.* **2014**, *19*, 131–136. [[CrossRef](#)] [[PubMed](#)]
- Busch, A.; Grimm, C.; Hartmann, E.; Paloschi, V.; Kickuth, R.; Lengquist, M.; Otto, C.; Eriksson, P.; Kellersmann, R.; Lorenz, U.; et al. Vessel wall morphology is equivalent for different artery types and localizations of advanced human aneurysms. *Histochem. Cell Biol.* **2017**, *148*, 425–433. [[CrossRef](#)] [[PubMed](#)]
- Abdul-Hussien, H.; Hanemaaijer, R.; Kleemann, R.; Verhaaren, B.F.; van Bockel, J.H.; Lindeman, J.H. The pathophysiology of abdominal aortic aneurysm growth: Corresponding and discordant inflammatory and proteolytic processes in abdominal aortic and popliteal artery aneurysms. *J. Vasc. Surg.* **2010**, *51*, 1479–1487. [[CrossRef](#)] [[PubMed](#)]
- Busch, A.; Pauli, J.; Winski, G.; Bleichert, S.; Chernogubova, E.; Metschl, S.; Winter, H.; Trenner, M.; Wiegering, A.; Otto, C.; et al. Lenvatinib halts aortic aneurysm growth by restoring smooth muscle cell contractility. *J. Clin. Investig.* **2021**, *6*, e140364. [[CrossRef](#)] [[PubMed](#)]
- King, K.E.; Iyemere, V.P.; Weissberg, P.L.; Shanahan, C.M. Kruppel-like factor 4 (KLF4/GKLF) is a target of bone morphogenetic proteins and transforming growth factor beta 1 in the regulation of vascular smooth muscle cell phenotype. *J. Biol. Chem.* **2003**, *278*, 11661–11669. [[CrossRef](#)]
- Riches-Suman, K.; Clark, E.; Helliwell, R.J.; Angelini, T.G.; Hemmings, K.; Bailey, M.A.; Bridge, K.I.; Scott, D.J.A.; Porter, K.E. Progressive Development of Aberrant Smooth Muscle Cell Phenotype in Abdominal Aortic Aneurysm Disease. *J. Vasc. Res.* **2018**, *55*, 35–46. [[CrossRef](#)]
- Moehle, C.W.; Bhamidipati, C.M.; Alexander, M.R.; Mehta, G.S.; Irvine, J.N.; Salmon, M.; Upchurch, G.R.; Kron, I.L.; Owens, G.K.; Ailawadi, G. Bone marrow-derived MCP1 required for experimental aortic aneurysm formation and smooth muscle phenotypic modulation. *J. Thorac. Cardiovasc. Surg.* **2011**, *142*, 1567–1574. [[CrossRef](#)]
- Jacob, T.; Schutze, R.; Hingorani, A.; Ascher, E. Differential expression of YAMA/CPP-32 by T lymphocytes in popliteal artery aneurysm. *J. Surg. Res.* **2003**, *112*, 111–116. [[CrossRef](#)] [[PubMed](#)]
- Hurks, R.; Kropman, R.H.; Pennekamp, C.W.; Hoefer, I.E.; de Vries, J.-P.P.; Pasterkamp, G.; Vink, A.; Moll, F.L. Popliteal artery aneurysms differ from abdominal aortic aneurysms in cellular topography and inflammatory markers. *J. Vasc. Surg.* **2014**, *60*, 1514–1519. [[CrossRef](#)] [[PubMed](#)]

24. Busch, A.; Hartmann, E.; Grimm, C.; Ergün, S.; Kickuth, R.; Otto, C.; Kellersmann, R.; Lorenz, U. Heterogeneous histomorphology, yet homogeneous vascular smooth muscle cell dedifferentiation, characterize human aneurysm disease. *J. Vasc. Surg.* **2017**, *66*, 1553–1564.e6. [[CrossRef](#)]
25. Pelisek, J.; Hegenloh, R.; Bauer, S.; Metschl, S.; Pauli, J.; Glukha, N.; Busch, A.; Reutersberg, B.; Kallmayer, M.; Trenner, M.; et al. Biobanking: Objectives, Requirements, and Future Challenges—Experiences from the Munich Vascular Biobank. *J. Clin. Med.* **2019**, *8*, 251. [[CrossRef](#)]
26. Ritchie, M.E.; Phipson, B.; Wu, D.; Hu, Y.; Law, C.W.; Shi, W.; Smyth, G.K. limma powers differential expression analyses for RNA-sequencing and microarray studies. *Nucleic Acids Res.* **2015**, *43*, e47. [[CrossRef](#)]
27. Assarsson, E.; Lundberg, M.; Holmquist, G.; Björkesten, J.; Thorsen, S.B.; Ekman, D.; Eriksson, A.; Dickens, E.R.; Ohlsson, S.; Edfeldt, G.; et al. Homogenous 96-Plex PEA Immunoassay Exhibiting High Sensitivity, Specificity, and Excellent Scalability. *PLoS ONE* **2014**, *9*, e95192. [[CrossRef](#)] [[PubMed](#)]
28. Lind, L.; Ärnlöv, J.; Lindahl, B.; Siegbahn, A.; Sundström, J.; Ingelsson, E. Use of a proximity extension assay proteomics chip to discover new biomarkers for human atherosclerosis. *Atherosclerosis* **2015**, *242*, 205–210. [[CrossRef](#)]
29. Subramanian, A.; Tamayo, P.; Mootha, V.K.; Mukherjee, S.; Ebert, B.L.; Gillette, M.A.; Paulovich, A.; Pomeroy, S.L.; Golub, T.R.; Lander, E.S.; et al. Gene set enrichment analysis: A knowledge-based approach for interpreting genome-wide expression profiles. *Proc. Natl. Acad. Sci. USA* **2005**, *102*, 15545–15550. [[CrossRef](#)]
30. Kanehisa, M.; Goto, S.; Kawashima, S.; Nakaya, A. The KEGG databases at GenomeNet. *Nucleic Acids Res.* **2002**, *30*, 42–46. [[CrossRef](#)]
31. Liberzon, A.; Birger, C.; Thorvaldsdottir, H.; Ghandi, M.; Mesirov, J.P.; Tamayo, P. The Molecular Signatures Database (MSigDB) hallmark gene set collection. *Cell Syst.* **2015**, *1*, 417–425. [[CrossRef](#)] [[PubMed](#)]
32. Fabregat, A.; Sidiropoulos, K.; Viteri, G.; Forner, O.; Marin-Garcia, P.; Arnaud, V.; D'eustachio, P.; Stein, L.; Hermjakob, H. Reactome pathway analysis: A high-performance in-memory approach. *BMC Bioinform.* **2017**, *18*, 142. [[CrossRef](#)]
33. Sachdeva, J.; Mahajan, A.; Cheng, J.; Baeten, J.T.; Lilly, B.; Kuivaniemi, H.; Hans, C.P. Smooth muscle cell-specific Notch1 haploinsufficiency restricts the progression of abdominal aortic aneurysm by modulating CTGF expression. *PLoS ONE* **2017**, *12*, e0178538. [[CrossRef](#)]
34. Rijbroek, A.; Moll, F.; Dijk, H.; Meijer, R.; Jansen, J. Inflammation of the abdominal aortic aneurysm wall. *Eur. J. Vasc. Surg.* **1994**, *8*, 41–46. [[CrossRef](#)] [[PubMed](#)]
35. Shiwani, H.; Baxter, P.; Taylor, E.; Bailey, M.A.; Scott, D.J.A. Modelling the growth of popliteal artery aneurysms. *Br. J. Surg.* **2018**, *105*, 1749–1752. [[CrossRef](#)]
36. Wågsäter, D.; Ravn, H.; Wanhainen, A.; Isaksson, H.; Björck, M. Circulating microRNA in patients with popliteal and multiple artery aneurysms. *JVS Vasc. Sci.* **2021**, *2*, 129–135. [[CrossRef](#)]
37. Busch, A.; Busch, M.; Scholz, C.-J.; Kellersmann, R.; Otto, C.; Chernogubova, E.; Maegdefessel, L.; Zernecke, A.; Lorenz, U. Aneurysm miRNA Signature Differs, Depending on Disease Localization and Morphology. *Int. J. Mol. Sci.* **2016**, *17*, 81. [[CrossRef](#)] [[PubMed](#)]
38. Serra, R.; Grande, R.; Montemurro, R.; Butrico, L.; Caliò, F.G.; Mastrangelo, D.; Scarcello, E.; Gallelli, L.; Buffone, G.; de Franciscis, S. The role of matrix metalloproteinases and neutrophil gelatinase-associated lipocalin in central and peripheral arterial aneurysms. *Surgery* **2015**, *157*, 155–162. [[CrossRef](#)]
39. Kershen, L.M.; Schucany, W.G.; Gilbert, N.F. Nora's lesion: Bizarre parosteal osteochondromatous proliferation of the tibia. *Proc. Bayl. Univ. Med. Cent.* **2012**, *25*, 369–371. [[CrossRef](#)]
40. Faggioli, G.L.; Gargiulo, M.; Bertoni, F.; Bacchini, P.; Gessaroli, M.; Stella, A. Parietal inflammatory infiltrate in peripheral aneurysms of atherosclerotic origin. *J. Cardiovasc. Surg.* **1992**, *33*, 331–336.
41. Akamatsu, D.; Fujishima, F.; Sato, A.; Goto, H.; Watanabe, T.; Hashimoto, M.; Shimizu, T.; Sugawara, H.; Miura, T.; Zukeran, T.; et al. Inflammatory Popliteal Aneurysm. *Ann. Vasc. Surg.* **2011**, *25*, 698.e13–698.e16. [[CrossRef](#)]
42. Busch, A.; Bleichert, S.; Ibrahim, N.; Wortmann, M.; Eckstein, H.-H.; Brostjan, C.; Wagenhäuser, M.U.; Goergen, C.J.; Maegdefessel, L. Translating mouse models of abdominal aortic aneurysm to the translational needs of vascular surgery. *JVS Vasc. Sci.* **2021**, *2*, 219–234. [[CrossRef](#)]
43. Johnson, S.C.; Dong, X.; Vijg, J.; Suh, Y. Genetic evidence for common pathways in human age-related diseases. *Aging Cell* **2015**, *14*, 809–817. [[CrossRef](#)] [[PubMed](#)]
44. Aboyans, V.; Ricco, J.B.; Bartelink, M.E.L.; Björck, M.; Brodmann, M.; Cohnert, T.; Collet, J.P.; Czerny, M.; De Carlo, M.; Debus, S.; et al. Editor's Choice—2017 ESC Guidelines on the Diagnosis and Treatment of Peripheral Arterial Diseases, in collaboration with the European Society for Vascular Surgery (ESVS). *Eur. J. Vasc. Endovasc. Surg.* **2018**, *55*, 305–368. [[CrossRef](#)] [[PubMed](#)]
45. Palazzuoli, A.; Gallotta, M.; Guerrieri, G.; Quatrini, I.; Franci, B.; Campagna, M.S.; Neri, E.; Benvenuti, A.; Sassi, C.; Nuti, R. Prevalence of risk factors, coronary and systemic atherosclerosis in abdominal aortic aneurysm: Comparison with high cardiovascular risk population. *Vasc. Health Risk Manag.* **2008**, *4*, 877–883. [[CrossRef](#)] [[PubMed](#)]
46. Ketelhuth, D.F.; Hansson, G.K. Adaptive Response of T and B Cells in Atherosclerosis. *Circ. Res.* **2016**, *118*, 668–678. [[CrossRef](#)]
47. Sakalihasan, N.; Michel, J.B.; Katsaryris, A.; Kuivaniemi, H.; Defraigne, J.O.; Nchimi, A.; Powell, J.T.; Yoshimura, K.; Hultgren, R. Abdominal aortic aneurysms. *Nat. Rev. Dis. Prim.* **2018**, *4*, 34. [[CrossRef](#)]

48. Michel, J.-B.; Martin-Ventura, J.-L.; Egido, J.; Sakalihasan, N.; Treska, V.; Lindholz, J.; Allaire, E.; Thorsteinsdottir, U.; Cockerill, G.; Swedenborg, J.; et al. Novel aspects of the pathogenesis of aneurysms of the abdominal aorta in humans. *Cardiovasc. Res.* **2011**, *90*, 18–27. [[CrossRef](#)]
49. Ruddy, J.M.; Jones, J.A.; Spinale, F.G.; Ikonomidis, J.S. Regional heterogeneity within the aorta: Relevance to aneurysm disease. *J. Thorac. Cardiovasc. Surg.* **2008**, *136*, 1123–1130. [[CrossRef](#)]
50. Lindsay, M.E.; Dietz, H.C. Lessons on the pathogenesis of aneurysm from heritable conditions. *Nature* **2011**, *473*, 308–316. [[CrossRef](#)]
51. Rickel, A.P.; Sanyour, H.J.; Kinser, C.; Khatiwada, N.; Vogel, H.; Hong, Z. Exploring the difference in the mechanics of vascular smooth muscle cells from wild-type and apolipoprotein-E knockout mice. *Am. J. Physiol. Physiol.* **2022**, *323*, C1393–C1401. [[CrossRef](#)]
52. Gomez, D.; Owens, G.K. Smooth muscle cell phenotypic switching in atherosclerosis. *Cardiovasc. Res.* **2012**, *95*, 156–164. [[CrossRef](#)]
53. Schwartz, S.M.; Virmani, R.; Majesky, M.W. An update on clonality: What smooth muscle cell type makes up the atherosclerotic plaque? *F1000Research* **2018**, *7*. [[CrossRef](#)] [[PubMed](#)]
54. Jacob, T.; Hingorani, A.; Ascher, E. Examination of the Apoptotic Pathway and Proteolysis in the Pathogenesis of Popliteal Artery Aneurysms. *Eur. J. Vasc. Endovasc. Surg.* **2001**, *22*, 77–85. [[CrossRef](#)]
55. Jacob, T.; Ascher, E.; Hingorani, A.; Gunduz, Y.; Kallakuri, S. Initial Steps in the Unifying Theory of the Pathogenesis of Artery Aneurysms. *J. Surg. Res.* **2001**, *101*, 37–43. [[CrossRef](#)]
56. Wilson, W.; Anderton, M.; Choke, E.; Dawson, J.; Loftus, I.; Thompson, M. Elevated Plasma MMP1 and MMP9 are Associated with Abdominal Aortic Aneurysm Rupture. *Eur. J. Vasc. Endovasc. Surg.* **2008**, *35*, 580–584. [[CrossRef](#)]
57. Petsophasakul, P.; Furmanik, M.; Forsythe, R.; Dweck, M.; Schurink, G.W.; Natour, E.; Reutelingsperger, C.; Jacobs, M.; Mees, B.; Schurgers, L. Role of Vascular Smooth Muscle Cell Phenotypic Switching and Calcification in Aortic Aneurysm Formation. *Arter. Thromb. Vasc. Biol.* **2019**, *39*, 1351–1368. [[CrossRef](#)]
58. Paloschi, V.; Sabater-Lleal, M.; Middelkamp, H.; Vivas, A.; Johansson, S.; van der Meer, A.; Tenje, M.; Maegdefessel, L. Organ-on-a-chip technology: A novel approach to investigate cardiovascular diseases. *Cardiovasc. Res.* **2021**, *117*, 2742–2754. [[CrossRef](#)]

**Disclaimer/Publisher's Note:** The statements, opinions and data contained in all publications are solely those of the individual author(s) and contributor(s) and not of MDPI and/or the editor(s). MDPI and/or the editor(s) disclaim responsibility for any injury to people or property resulting from any ideas, methods, instructions or products referred to in the content.